ELSEVIER

Materials Science and Engineering B 117 (2005) 123–128

MATERIALS SCIENCE & ENGINEERING B

www.elsevier.com/locate/mseb

Structure and electrochemical characteristics of $RENi_3$ alloy

Xinbo Zhang, Wenya Yin, Yujun Chai, Minshou Zhao*

Graduate School of the Chinese Academy of Sciences, Key Laboratory of Rare Earth Chemistry and Physics, Changchun Institute of Applied Chemistry, Chinese Academy of Sciences, Changchun 130022, PR China

Received 21 September 2004; received in revised form 1 November 2004; accepted 4 November 2004

Abstract

The $RENi_3$ (RE = La, Ce, Pr, Nd, Sm, Gd, Tb, Dy, Ho, Er, Y) series compounds have been prepared by arc melting constituent elements under Ar atmosphere. X-ray diffraction (XRD) analysis reveals that the as-prepared alloys have different lattice parameters and cell volumes, depending on different rare earth (RE) element. The electrochemical characteristics, including the electrochemical capacity, P–C isotherms, high rate chargeability (HRC) and high-rate dischargeability (HRD), of these alloys have been studied through the charge-discharge recycle testing at different temperatures, charge currents and discharge currents. The results show that YNi_3 has the largest cell volume, smallest density, and moreover, it shows more satisfactory electrochemical characteristics than other alloys, including discharge capacity, HRC, HRD and low temperature dischargeablity.

Keywords: Metal hydride electrode; Ni-MH battery; P–C isotherms; Electrochemical characteristic; Rare earth element

1. Introduction

Recently, secondary batteries with high energy density and long durability are urgently required as a power source for portable appliances and zero emission vehicles. Due to a high specific energy, a high resistance to overcharging and overdischarging, capability of performing high rate charge/discharge, environmental friendliness, and interchangeability with the nickel-cadmium battery, the nickel-metal hydride (Ni-MH) battery has been widely investigated and applied in portable telecommunication equipment, electric tools and electric vehicles [1–3]. The Negative electrodes are the most important component in a Ni-MH battery.

AB_5 alloys, where A represents a metal that is capable of reacting exothermically with hydrogen and forming a stable hydride and B represents another kind of metal which cannot form a stable hydride but can catalyze the hydrogen reaction, are generally employed as the negative electrode material in nickel-metal hydride battery. The AB_5 type alloy has been studied extensively as the negative electrode material in Ni-MH battery [4,5], because it can easily react with hydrogen at normal temperatures and is chemical stable. However, the capacity of AB_5 type alloys is almost approaching its technical limitation nowadays because the repeated improvements to increase the capacity have already realized very high utilization of the intrinsic capacity of the alloy, and further increases in discharge capacity will be difficult.

The structure of an AB_3 compound (PuNi3-type) is obtained by combining the AB_5 with AB_2 units [$AB_5 + 2(AB_2) = 3(AB_3)$] [6]. From the viewpoint of gas-solid reactions, Oesterreicher et al. [7,8] and Takeshita et al. [9,10] have studied the hydriding characteristics of $LaNi_3$ and RT_3 phases (R = Dy, Ho, Er, Tb, Gd; T = Fe or Co), respectively. Their results showed that the hydrogen storage capacity of the AB_3 type alloy exceeds that of the well-known hydrogen storage AB_5 type alloy, which indicates that AB_3 alloy is a potential candidate for the negative electrode material. Nevertheless, it was pointed out that AB_3 type alloy is subject to the problem that the stored hydrogen in the $LaNi_3$ alloy is released sparingly after absorption [11]. Although there have been some studies on AB_3 compounds, the results are still quite incomplete. Moreover, the electrode characteristics of these alloys have been hardly investigated [12]. This study, as a part of the research work in our group, concerns the use of $RENi_3$ (RE = La, Ce, Pr, Nd, Sm, Gd, Tb, Dy, Ho, Er, Y) hydrogen

* Corresponding author. Tel.: +86 431 5262365; fax: +86 431 5262365.
E-mail address: zhaoms@ciac.jl.cn (M. Zhao).

0921-5107/$ – see front matter © 2004 Elsevier B.V. All rights reserved.
doi:10.1016/j.mseb.2004.11.017

storage alloys as the negative electrode material in a Ni-MH battery.

2. Experimental details

2.1. Alloy preparation and X-ray diffraction analysis

All alloy samples were prepared by arc-melting the constituent elements or master alloy on a water-cooled copper hearth under an argon atmosphere followed by annealing in vacuum for 20 h at 770 °C. The purity of the metals, i.e., La, Ce, Pr, Nd, Sm, Gd, Tb, Dy, Ho, Er, Y, Ni, is higher than 99.9 mass%. The samples were all inverted and remelted five times to ensure good homogeneity. These alloy samples were then crushed in mortar into fine powders of 200–300 mesh.

Crystallographic characteristics of the hydrogen storage alloys were investigated by X-ray diffraction (XRD) using a Rigaku D/Max 2500PC X-ray diffractometer (Cu Ka, graphite monochromator) and JADE5 software [13]. The lattice constants and cell volume were calculated by the cell program [14] after internal theta calibration using silicon as the standard reference material.

2.2. Electrochemical measurements

The well-mixed alloy powder and carbonyl nickel powder in a weight ratio of 1:5 were pressed into tablets for the metal hydride electrode, with dimensions of 13 mm diameter, thickness of 1.5 mm. The weight of each electrode was about 0.9 g.

The electrochemical properties were then measured in a standard three electrode cell consisting of a working electrode (metal hydride electrode), a counter-electrode ($NiOOH/Ni(OH)_2$ electrode) and a reference electrode (Hg/HgO). The electrolyte in the cell was 6 M KOH aqueous solution. Charge and discharge tests were carried out on a DC-5 battery testing instrument controlled by computer. The emphasis of these charge/discharge tests was on the electrochemical capacity and stability of the negative electrode, thus the capacity of the positive electrode plate was designed to be much higher than that of the negative electrode. These experimental cells were first charged at 293 K at a current of 60 mA g^{-1} for 5.5 h, then rested for 30 min before discharging at the same discharge current density to the cut off voltage of −0.60 V versus Hg/HgO.

P–C–T curves were electrochemically obtained by converting the equilibrium potential of the metal hydride to the equilibrium pressure of hydrogen on the basis of Nernst equation using electrochemical data [15] as reported in reference [16]. The equilibrium potential curves were obtained by alternating the following two processes: (1) a pulse discharge of (25 mA g^{-1} × 0.25 h) and (2) a rest period until the potential became almost constant. The equilibrium potential change of approximately 30 mV corresponds to the equilibrium pressure change by one order of magnitude. Since the measured potentials have an error of 1–2 mV, the calculated pressure values are accurate to within 10% [16].

To evaluate the high rate dischargeability (HRD) (in the range of 90–900 mA g^{-1}), the charging current density was kept constant at 60 mA g^{-1} and the obtained discharge capacity was denoted as C_i. On the other hand, when the high rate chargeability (HRC) (90–900 mA g^{-1}) was investigated, the discharge current density was held at 60 mA g^{-1} and thus we got the discharge capacity (C_j). HRD (or HRC) are generally defined as the ratio of the discharge capacity C_i (or C_j) at the cut off voltage of −0.6 V to the maximum capacity C_{max}, namely: $HRD = C_i/C_{max} \times 100\%$, $HRC = C_j/C_{max} \times 100\%$, respectively.

For investigating the electrocatalytic activity of the hydrogen electrode reaction, the linear polarization curves of the electrode were plotted on a EG&G PARC's Model 273 Potentiostat/Galvanostat station by scanning the electrode potential at the rate of 0.1 mV/s from −5 to 5 mV (versus open circuit potential) at 50% depth of discharge (DOD) at 293 K. The polarization resistance R_p can be obtained from the slope of the linear polarization curves. Moreover, the exchange current density (I_0), which is a measure of the catalytic activity of electrode, was calculated from the slopes of polarization curves by the following equation [17]

$$I_0 = \frac{RT}{FR_P}$$

where R is the gas constant; T, the absolute temperature; F, the Faraday constant; and R_p, the polarization resistance. The potentiostatic discharge technique was used to evaluate the coefficient of diffusion within the bulk of the alloy electrodes. After being fully charged followed by a 30 min open-circuit lay-aside, the test electrodes were discharged with +500 mV potential-step for 500 s on a EG&G PARC's Model 273 Potentiostat/Galvanostat station, using the M352 CorrWare electrochemical/corrosion software.

The hydride electrodes were charged at different temperatures (T = 233, 253, 293, 333 K) (the charged capacity was represented by C_c) and then discharged at 293 K to determine the dependence of charge efficiency on temperature (the obtained discharge capacity was denoted as C_d). The charge efficiency was defined as the ratio of the discharge capacity C_d at the cutoff voltage of −0.6 v to the charge capacity C_c. In contrast if they were charged at 293 K and discharged at various temperatures, the discharge efficiency can be evaluated.

3. Results and discussion

3.1. Structure characteristics

Fig. 1 shows the XRD patterns of the alloys with different chemical compositions. The results indicate that these alloys all are homogenous with a single phase corresponding to a hexagonal $PuNi_3$ type structure. Careful examination of the diffraction angle reveals a peak shift upon changing the com-

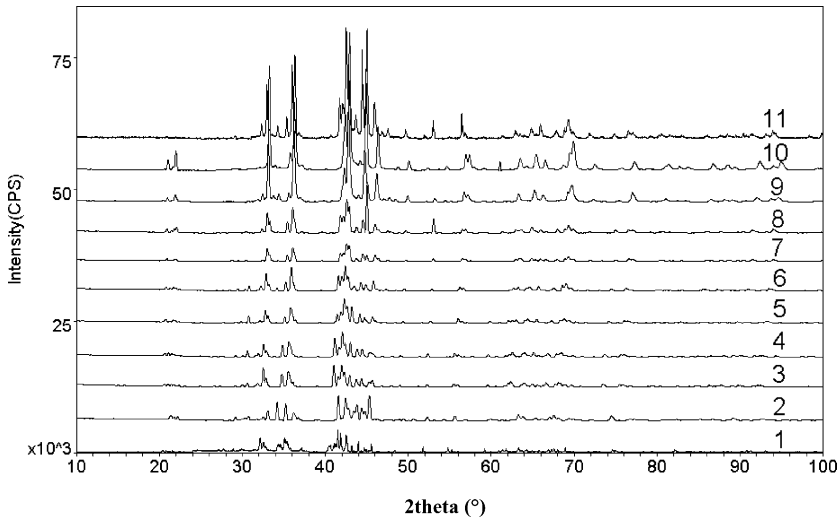

Fig. 1. X-ray diffraction patterns of $RENi_3$ alloys (1: $LaNi_3$, 2: $CeNi_3$, 3: $PrNi_3$, 4: $NdNi_3$, 5: $SmNi_3$, 6: $GdNi_3$, 7: $TbNi_3$, 8: $DyNi_3$, 9:$HoNi_3$, 10: $ErNi_3$, 11: YNi_3).

position. The lattice parameters, cell volumes, and density of these alloys are listed in Table 1. It was found that both the lattice parameter and the cell volume change with the atomic radius of the rare earth (RE) elements in $RENi_3$ alloys. To demonstrate, further, the effect of atomic radius on the cell volume, density and discharge capacity, those parameters are plotted as a function of the atomic radius of rare earth element in Fig. 2. It can be clearly seen that both the cell volume and the density do not vary monotonically with increasing atomic radius of RE elements. YNi_3 has the largest cell volume and the smallest density among these alloys.

3.2. P–C isotherms

The electrochemical method is very useful for examining the charging and discharging levels of hydrogen in an anode, although the calculated pressures pertain to a quasi-equilibrium state [17]. The P–C isotherms (PCT) of hydrogen absorption and desorption for hydrogenated YNi_3 and $LaNi_3$ compounds at 293 K are presented in Fig. 3. It should be noted that $LaNi_3$ alloy shows a low desorption plateau pressure and a large hysteresis for the absorption–desorption pressure. YNi_3, however, shows an upper and flatter pressure plateau. This means that the substitution of Y for La favors the formation of a wider plateau and thus improves the electrochemical characteristics of the metal hydride electrode.

Table 1
Lattice parameter, cell volume and density for $RENi_3$ alloys

Alloy composition	Lattice parameter		Cell volume ($Å^3$)	Density (g/cm^3)
	a (Å)	c (Å)		
$LaNi_3$	5.087	25.018	560.67	8.359
$CeNi_3$	5.095	25.038	562.83	8.397
$PrNi_3$	5.075	25.077	559.27	8.471
$NdNi_3$	5.075	25.076	559.42	8.558
$SmNi_3$	5.077	25.056	559.36	8.723
$GdNi_3$	5.094	24.979	561.44	8.873
$TbNi_3$	5.07	25.227	561.55	8.916
$DyNi_3$	5.069	25.267	562.47	8.997
$HoNi_3$	5.095	25.076	563.75	9.041
$ErNi_3$	5.072	25.223	561.54	9.138
YNi_3	5.074	25.293	563.88	7.023

3.3. Activation and maximum discharge capacity

When the hydrogen storage alloy electrode is first charged, the stored hydrogen in the alloy is released sparingly after absorption. The process in which the freshly formed hydride electrodes are continuously charged and discharged in order

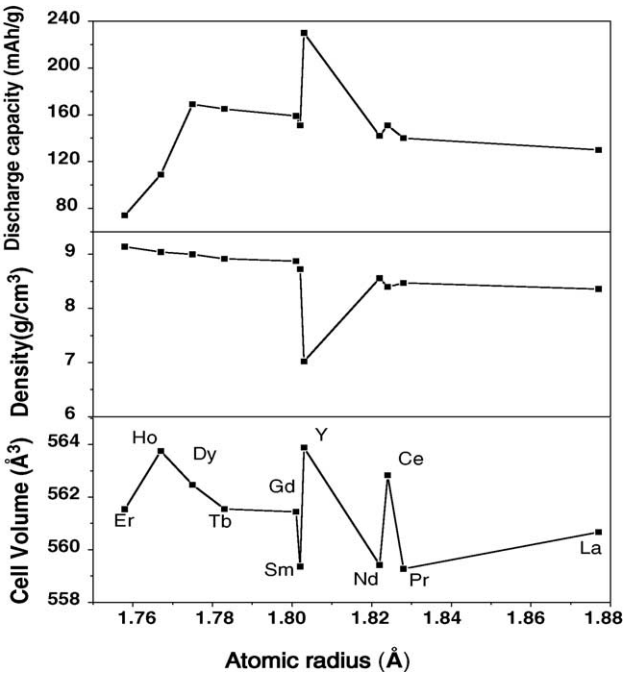

Fig. 2. Variations of unit cell volume, density and discharge capacity atomic radius of rare elements in $RENi_3$ compounds.

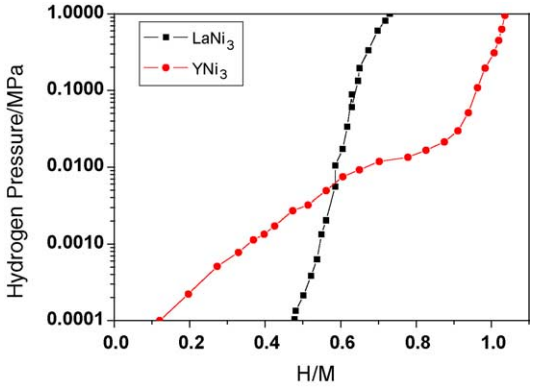

Fig. 3. Comparison of P–C–T isotherms for LaNi and YNi anode.

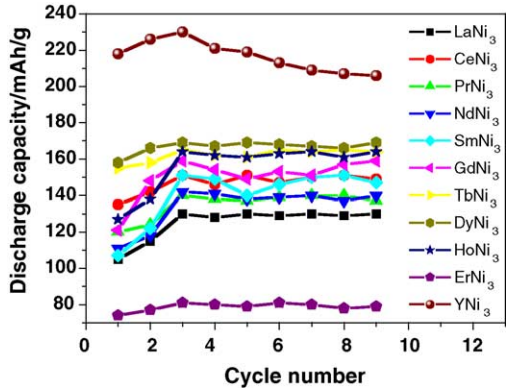

Fig. 4. Specific discharge capacity versus number of charge/discharge cycles of $RENi_3$ anodes.

to obtain the maximum electrochemical capacity is called activation. This is important for practical use of Ni-MH battery. Fig. 4 shows the activation profiles of the $RENi_3$ electrodes. The results show that the activation of all the alloy electrodes only needs three cycles, which means that $RENi_3$ alloy electrodes can easily be activated.

The maximum discharge capacity of $RENi_3$ electrodes at 293 K are shown in Figs. 2 and 4. Among these different alloy electrodes, YNi_3 has the largest specific capacity (230 mAh g^{-1}, 293 K, discharge current of 60 mA g^{-1}), which is more than 1.77 times than that of $LaNi_3$ (130 mAh g^{-1}). To understand why is so, the cell volume and density of the alloy must be considered. It can be seen in Table 1 and Fig. 2 that cell volume of YNi_3 is larger than that of other alloys, therefore it has the largest interstitial positions in the lattice, which will be beneficial to the hydrogen storage process. Moreover, the density of YNi_3 is the smallest of all the alloys. It is well known that the discharge capacity of alloy electrode is increased with decreasing density of alloy as long as the amount of uptake hydrogen atoms remains constant. On the other hand, $ErNi_3$ has the smallest discharge capacity because it has the highest density.

3.4. High rate chargeability and dischargeability

As an important kinetics property of the hydride electrode in battery, it is very important to minimize the decrease in discharge capacity even at the high charge/discharge current density. The HRC and HRD of the alloy electrodes for a discharge current density of 900 mA g^{-1} have been determined and are listed in Table 2. For brevity, only typical data for the $LaNi_3$ and YNi_3 are plotted in Fig. 5. As expected, the discharge capacity (taking the capacity at a discharge rate of

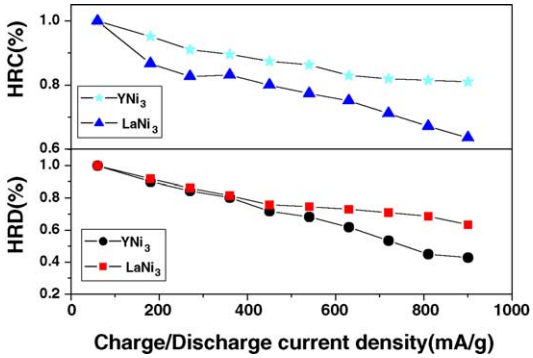

Fig. 5. The dependence of discharge capacity on the charge/discharge current density.

Table 2
Relationship between the HRC, HRD and cell volume of the $RENi_3$ alloys

Alloy composition	Cell volume (Å^3)	HRC (%)		HRD (%)	
		60 mA g^{-1}	900 mA g^{-1}	60 mA g^{-1}	900 mA g^{-1}
$PrNi_3$	559.27	100	51.7	100	32.5
$SmNi_3$	559.36	100	52	100	32.8
$NdNi_3$	559.42	100	52.3	100	33.1
$LaNi_3$	560.67	100	54.56	100	34.96
$GdNi_3$	561.44	100	57.1	100	36.1
$ErNi_3$	561.54	100	58.1	100	37.9
$TbNi_3$	561.55	100	58.6	100	38.2
$DyNi_3$	562.47	100	60.1	100	40.1
$CeNi_3$	562.83	100	65.1	100	46.3
$HoNi_3$	563.75	100	76.45	100	60.1
YNi_3	563.88	100	81	100	63.42

Table 3
The electrochemical kinetic parameters of $RENi_3$ alloy electrodes at 293 K

Alloy composition	Exchange current density, I_0 (mA g^{-1})	Hydrogen diffusion coefficient, D ($\times 10^{-10}$(cm^2/s))
$PrNi_3$	208.71	4.51
$SmNi_3$	209.13	5.26
$NdNi_3$	207.37	6.27
$LaNi_3$	209.46	7.14
$GdNi_3$	210.24	7.9
$ErNi_3$	206.72	9.21
$TbNi_3$	212.31	11
$DyNi_3$	208.33	11.94
$CeNi_3$	209.72	12.43
$HoNi_3$	213.11	13.11
YNi_3	215.27	14.69

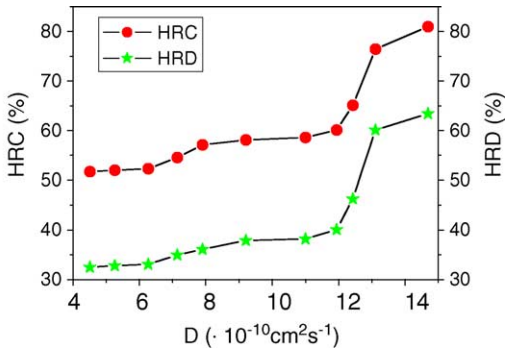

Fig. 6. The HRC and HRD as a function of hydrogen diffusion coefficient (D) of the $RENi_3$ alloy electrodes at 293 K.

60 mA g^{-1} as unity) decays with an increase in the charging current density. However, the YNi_3 alloy shows a better discharge capacity than the $LaNi_3$ alloy. For example, at a charge/discharge current of 900 mA g^{-1}, HRC and HRD of YNi_3 are 81, 63.42%, respectively, but the HRC and HRD of $LaNi_3$ are only 54.56, 34.96%, respectively. It is well known that the HRC and HRD of metal hydride electrode are influenced mainly by the electrochemical reaction kinetics on the alloy powder surface and the diffusion rate of hydrogen in the bulk of the alloy [17]. To examine the effect of the different rare earth elements on the charge and discharge kinetics, linear polarization and potentiostatic discharge technique were performed on these alloy electrodes and values obtained for the exchange current density I_0 and hydrogen diffusion coefficient for the $RENi_3$ alloy electrodes. The exchange current density I_0 and hydrogen diffusion coefficient for all $RENi_3$ alloy electrodes are summarized in Table 3. The exchange current density I_0 is not changed significantly (I_0 = 50.2–49.6%) between the different $RENi_3$ alloy electrodes. This is mainly ascribed to the similar chemical properties of the different rare earth elements. The similar exchange current densities of the alloy electrodes implies that surface reaction kinetics might not be as important as diffusion process for $RENi_3$ alloys as far as the HRC and HRD are concerned. The HRC and HRD as a function of hydrogen diffusion coefficient (D) of $RENi_3$ alloy electrodes are shown in Fig. 6. It is found that the HRC and HRD monotonically increase with an increase in D. The cell volume of YNi_3 is larger than that of $LaNi_3$, as shown in Table 1, which will beneficial to the hydrogen diffusion coefficient and thus a reasonable increase in HRC and HRD would be expected. The HRC, HRD and cell volume of $RENi_3$ alloys shown in Table 2 confirm the above explanation and also agree well with the data of Chang et al. [18].

3.5. Temperature effects

Alloys used as the negative electrode material in a Ni-MH battery should be capable of working at wide temperature range. Fig. 7 shows the discharge abilities of $LaNi_3$ and YNi_3 at different temperatures. It can be readily seen that the discharge capacities are sensitive to temperature. The electrodes reach their maximum discharge capacities at room temperature (293 K), and then decrease sharply with both on decrease or increase in temperature. For instance, both $LaNi_3$ and YNi_3 alloy electrodes can only discharge less than 60% of their maximum capacity at a high temperature (333 K). Actually, all the $RENi_3$ alloy electrodes have poor high temperature discharge capacities. Fig. 6 also shows that the low temperature discharge ability of the YNi_3 is better than that of $LaNi_3$ alloy electrode. The low temperature discharge ability is mainly controlled by hydrogen diffusion, and hydrogen can diffuse more easily in the bulk of alloys with a larger cell volume. Thus, the larger cell volume of YNi_3 than that of $LaNi_3$ doubtlessly results in its superior discharge ability at low temperature. However, owing to the larger cell volume, hydrogen evolution will become easier during charging, and the rates of self-discharge will become larger during discharge, and the specific capacity at high temperature will surely decrease with an increase of the cell volume. The high temperature discharge ability of YNi_3 should be improved to meet any extended application.

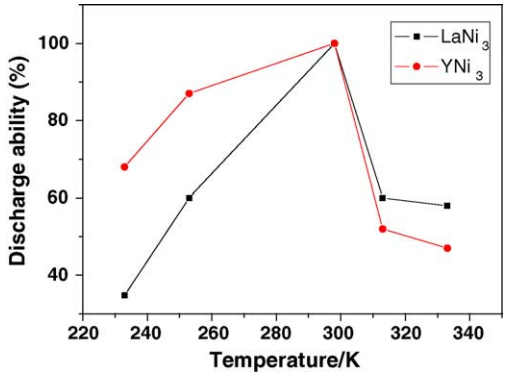

Fig. 7. Discharge ability of $LaNi_3$ and YNi_3 as the function of temperature at the discharge current of 60 mA g^{-1}.

4. Conclusions

The structure and electrochemical characteristics of $RENi_3$ (RE = La, Ce, Pr, Nd, Sm, Gd, Tb, Dy, Ho, Er, Y) type hydrogen storage alloys have been investigated in detail. It is found that YNi_3 has the largest cell volume, smallest density, and moreover, shows more satisfactory electrochemical characteristics than the other alloys, including discharge capacity, HRC, HRD and low temperature dischargeablity.

Acknowledgements

This work was financially supported by the National Natural Science Foundation of China (Grant No.20171042).

References

[1] S.R. Ovshinsky, M.A. Fetcenko, J. Ross, Science 260 (1993) 176.
[2] P. Gifford, J. Adams, D. Corrigan, S. Venkatesan, J. Power Sources 80 (1999) 157.
[3] F. Haschka, W. Warthmann, G. Benczru-Urmossy, J. Power Sources 72 (1998) 32.
[4] H. Oesterreicher, J. Clinton, H. Bittner, Mater. Res. Bull. 2 (1976) 1241.
[5] H. Miyamura, T. Sakai, K. Oguro, A. Kato, H. Ishikawa, J. Less-Common Met. 146 (1989) 197.
[6] B.D. Dump, P.J. Viccaro, G.K. Shenoy, J. Less-Common Met. 74 (1980) 75.
[7] H. Oesterreicher, J. Clinton, H. Bittner, Mater. Res. Bull. 11 (1974) 2282.
[8] H. Oesterreicher, K. Ensslen, A. Kerlin, E. Bucher, Mater. Res. Bull. 15 (1980) 275.
[9] T. Takeshita, W.E. Wallace, R.S. Craig, Inorg. Chem. 13 (1974) 2282.
[10] C.A. Bechman, A. Goudy, T. Takeshita, W.E. Wallace, R.S. Craig, Inorg. Chem. 15 (1976) 2184.
[11] J. Chen, H.T. Takeshita, H. Tanaka, N. Kuriyama, T. Sakai, I. Uehara, M. Haruta, J. Alloys Compd. 302 (2000) 304.
[12] J. Chen, N. Kuriyama, H.T. Takeshita, H. Tanaka, T. Sakai, M. Haruta, Electrochem. Solid-State Lett. 3 (6) (2000) 249.
[13] Materials Data JADE Release 5, XRD pattern processing, Materials Data Inc. (MDI), 1997.
[14] Y. Takaki, T. Taniguchand, K. Hori, J. Ceram. Soc. Jpn. Int. Ed. 97 (1993) 362.
[15] J. Balej, Int. J. Hydrogen Energy 10 (1985) 365.
[16] C. Iwakura, T. Asaoka, H. Yoneyama, T. Sakai, K. Oguro, H. Ishikawa, Nippon Kagaku Kaishi 8 (1988) 1482.
[17] T. Sakai, H. Miyamura, N. Kuriyama, A. Kato, K. Oguro, H. Ishikawa, J. Less-Common Met. 159 (1990) 127.
[18] J.K. Chang, D.S. Shong, W. Tsai, Mater. Chem. Phys. 83 (2004) 361.